
Perception-based Seam-cutting for Image Stitching

Nan Li · Tianli Liao · Chao Wang

Received: xxx / Accepted: xxx

Abstract Image stitching is still challenging in consumer-level photography due to imperfect image captures. Recent works show that seam-cutting approaches can effectively relieve the artifacts that generated by local misalignment. Normally, the seam-cutting approach is described in terms of energy minimization. However, few of existing methods consider the human perception in their energy functions, which sometimes causes that there exists another seam that is perceptually better than the one with the minimum energy. In this paper, we propose a novel perception-based seam-cutting approach that considers the nonlinearity and the nonuniformity of human perception into the energy minimization. Our method uses a sigmoid metric to characterize the perception of color discrimination and a saliency weight to simulate that the human eye inclines to pay more attention to the salient objects. In addition, our approach can be easily integrated into other stitching pipelines. Representative experiments demonstrate substantial improvements over the conventional seam-cutting approach.

Keywords Image stitching · Seam-cutting · Human perception · Energy minimization

1 Introduction

Image stitching is a well studied topic in computer vision and graphics [13, 29, 30], which mainly consists of align-

N. Li
Center for Applied Mathematics, Tianjin University, Tianjin 300072, China. E-mail: nan@tju.edu.cn

T. Liao (Corresponding author)
Center for Combinatorics, Nankai University, Tianjin 300071, China. E-mail: liaotianli@mail.nankai.edu.cn

C. Wang
Department of Software, Nankai University, Tianjin 300071, China. E-mail: wangchao@nankai.edu.cn

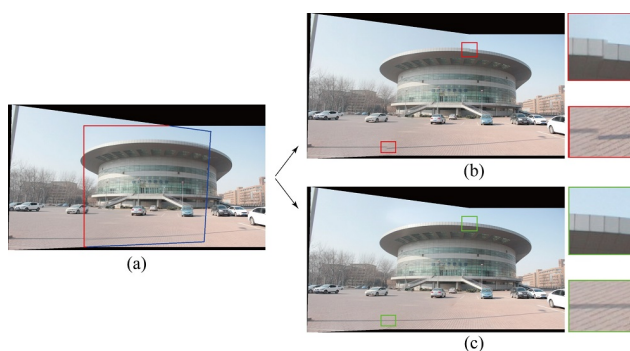


Fig. 1 A stitching result comparison between different seam-cutting approaches. **a** Overlapping region. **b** Stitching result corresponding to the conventional seam-cutting approach. **c** Stitching result corresponding to our perception-based seam-cutting approach.

ment [4, 8, 15, 31, 32, 34, 35], composition [9, 10, 12, 21, 26] and blending [6, 7, 17, 21, 22, 28]. In consumer-level photography, it is difficult to achieve perfect alignment due to unconstrained shooting environment. Thus, image composition becomes the most crucial step to produce artifacts-free stitching results.

The seam-cutting approach [1, 11, 18, 20, 37] is a powerful composition method, which intends to find an invisible seam in the overlapping region of the aligned images. Existing methods usually express the problem in terms of energy minimization and minimize it via graph-cut optimization [2, 3, 19]. Normally, for a given overlapping region of the aligned images, different energy functions correspond to different seams, and certainly correspond to different stitching results (Fig. 1). Conversely, in order to obtain a plausible stitching result, we desire to define a perception-based energy function such that the perceptually best seam has the minimum energy.

In recent years, many efforts have been devoted to seam-cutting by penalizing the photometric difference using vari-

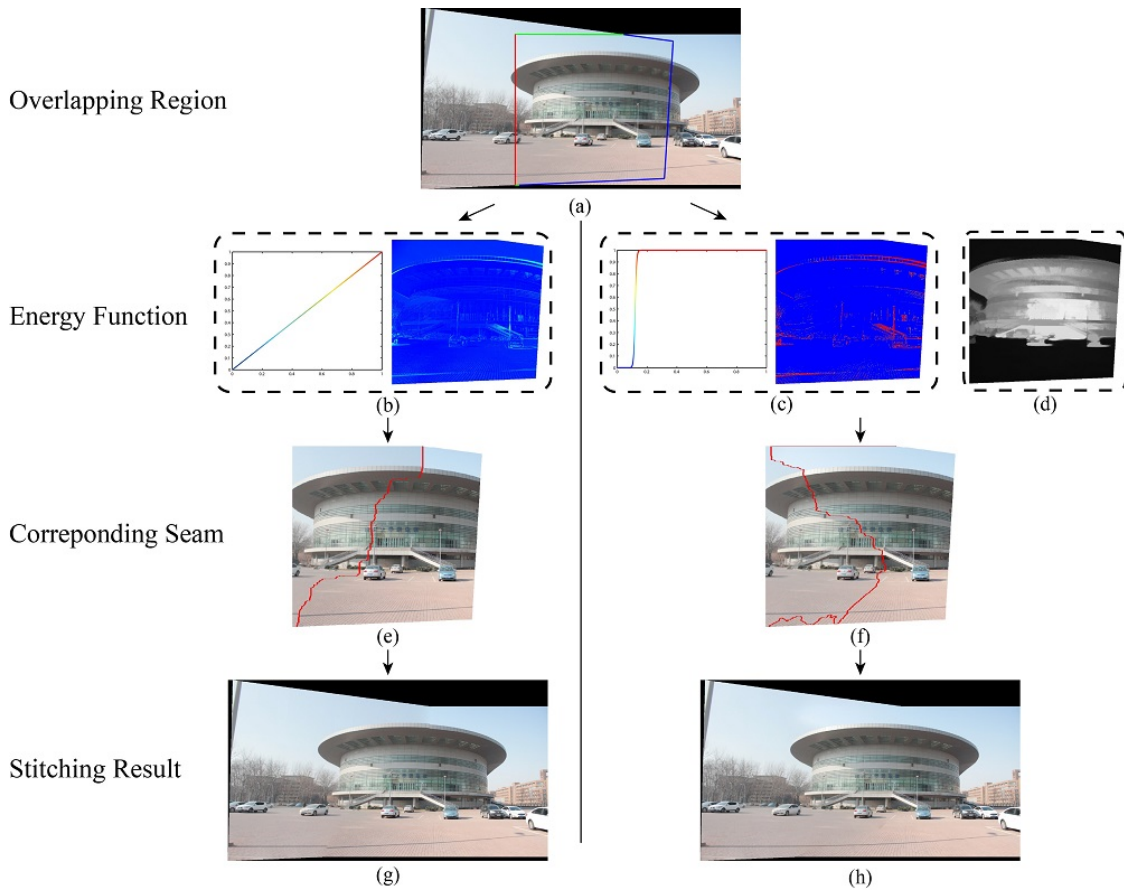


Fig. 2 A process comparison between the conventional and our perception-based seam-cutting approaches. **a** Overlapping region. **b** Euclidean-metric color difference. **c** Sigmoid-metric color difference. **d** Average pixel saliency. **e, f** Corresponding seams. **g, h** Corresponding stitching results.

ous energy functions. The Euclidean-metric color difference is used in [20] to define the smoothness term in their energy function and the gradient difference is taken into account in [1]. Eden *et al.* [11] proposed an energy function that allows for large motions and exposure differences, but the camera setting is required. Jia and Tang [18] associated the smoothness term with the gradient smoothness and the gradient similarity to reduce the structure complexity along the seam. Zhang *et al.* [37] combined the alignment errors and the Gaussian-metric color difference in their energy function to handle misaligned areas with similar colors. However, few of existing methods consider the human perception in their energy functions, which sometimes causes that there exists another seam that is perceptually better than the one with the minimum energy.

The seam-cutting approach has also been applied in image alignment. Gao *et al.* [16] proposed a seam-driven image stitching framework, which finds the best homography warp from some candidates with the minimal seam cost instead of the one with the minimal alignment error. Zhang and Liu [36] combined homography and content-preserving warps [24] to locally align the images, where the seam cost is used as a quality metric to predict how well a homog-

raphy warp enables plausible stitching. Lin *et al.* [23] proposed a seam-guided local alignment, which iteratively improves warping by adaptive feature weighting according to their distances to the current seam.

In this paper, we propose a novel perception-based seam-cutting approach that considers the nonlinearity and the nonuniformity of human perception into the energy minimization. Our proposed method consists of three stages (Fig. 2). In the first stage, we calculate the sigmoid-metric color difference of the given overlapping region as the smoothness term to characterize the perception of color discrimination. Then, we calculate the average pixel saliency of the given overlapping region as the saliency weight to simulate that the human eye inclines to pay more attention to the salient objects. Finally, we minimize the perception-based energy function by the graph-cut optimization to obtain the seam and the corresponding stitching result.

Experiments demonstrate that our perception-based seam-cutting approach outperforms the conventional seam-cutting approach. A user study shows that our stitching results are more consistent with the human perception.

Major contributions of the paper are summarized as follows.

1. We proposed a perception-based seam-cutting approach to create nearly perception-consistent stitching results.
2. Our approach can be easily integrated into other stitching pipelines.

2 Approach

In this section, we first show more details of the conventional seam-cutting approach, then propose the perception-based energy function, finally summarize our seam-cutting framework.

2.1 Conventional seam-cutting approach

Given a pair of aligned images denoted by I_0 and I_1 , let \mathbf{P} be their overlapping region and $\mathbf{L} = \{0, 1\}$ be a label set, where “0” corresponds to I_0 and “1” corresponds to I_1 , then a seam means assigning a label $l_p \in \mathbf{L}$ to each pixel $p \in \mathbf{P}$. The goal of seam-cutting approaches is to find a labeling l (i.e., a map from \mathbf{P} to \mathbf{L}) that minimizes the energy function

$$E(l) = \sum_{p \in \mathbf{P}} D_p(l_p) + \sum_{(p,q) \in \mathbf{N}} S_{p,q}(l_p, l_q), \quad (1)$$

where $\mathbf{N} \subset \mathbf{P} \times \mathbf{P}$ is a neighborhood system of pixels. The *data term* $D_p(l_p)$ represents the cost of assigning a label l_p to a pixel $p \in \mathbf{P}$, and the *smoothness term* $S_{p,q}(l_p, l_q)$ represents the cost of assigning a pair of labels (l_p, l_q) to a pair of pixels $(p, q) \in \mathbf{N}$.

The data term is defined as

$$\begin{cases} D_p(1) = 0, D_p(0) = \mu, & \text{if } p \in \partial I_0 \cap \partial \mathbf{P}, \\ D_p(0) = 0, D_p(1) = \mu, & \text{if } p \in \partial I_1 \cap \partial \mathbf{P}, \\ D_p(0) = D_p(1) = 0, & \text{otherwise,} \end{cases} \quad (2)$$

where μ is a very large penalty to avoid mislabeling, $\partial I_k \cap \partial \mathbf{P}$ is the common border of I_k ($k = 0, 1$) and \mathbf{P} respectively (Fig. 1a). In fact, the data term $D_p(l_p)$ fixes the endpoints of the seam as the intersections of the two colored polylines (Fig. 2e).

The smoothness term is defined as

$$S_{p,q}(l_p, l_q) = \frac{1}{2} |l_p - l_q| (I_*(p) + I_*(q)), \quad (3)$$

$$I_*(\cdot) = \|I_0(\cdot) - I_1(\cdot)\|_2, \quad (4)$$

where $I_*(\cdot)$ denotes the Euclidean-metric color difference.

The energy function (1) is minimized by the graph-cut optimization to obtain the seam and the stitching result (Fig. 1b). Obviously, the definition of the energy function plays the most important role in the seam-cutting approach.

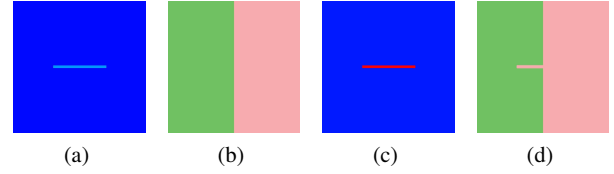


Fig. 3 Toy example. **a,c** Visualizations of the Euclidean-metric and the sigmoid-metric color difference. **b,d** Corresponding seams.

2.2 Perception-based energy function

In the experiments, there may exist another seam l_{\dagger} that is perceptually better than the seam l_* that minimizes the energy function (1). Therefore, we desire to define a perception-based energy function such that the perceptually best seam has the minimum energy.

2.2.1 Sigmoid metric

Fig. 3 shows a toy example where l_* is not perceptually best. In fact, the seam l_* shown in **b** crosses the local misalignment area (marked in light blue in **a**), because the Euclidean-metric color difference does not give it a large enough penalty. In contrast, the seam l_{\dagger} shown in **d** avoids the local misalignment area (marked in red in **c**), because the sigmoid-metric color difference successfully distinguishes it from the alignment area.

In particular, the perception of colors is nonlinear as it has a color discrimination threshold, which means that the human eye cannot differentiate some colors from others even if they are different. Let τ denote the threshold, the perception of color discrimination can be characterized as

- if $I_*(\cdot) < \tau$, color difference is invisible,
- if $I_*(\cdot) \approx \tau$, sensitivity of discrimination rises rapidly,
- if $I_*(\cdot) > \tau$, color difference is visible.

We want to define a quality metric to measure the visibility of color difference such that the cost of invisible terms approximates zero while the cost of visible terms approximates one. Fortunately, the sigmoid function

$$\text{sigmoid}(x) = \frac{1}{1 + e^{-4\kappa(x-\tau)}}, \quad (5)$$

is a suitable quality metric for our purpose.

Now we explain how to determine the parameters τ and κ . Briefly, given an overlapping region \mathbf{P} of the aligned images, the threshold τ plays the role for roughly dividing \mathbf{P} into an alignment area and a misalignment area by the color difference, which is very similar to determine a threshold to divide a gray image into a background region and a foreground region. Thus, we employ the well-known Ostu’s algorithm [27] to determine a suitable τ with the maximum between-class variance. On the other hand, κ represents how rapidly the sensitivity of color discrimination rises around τ .

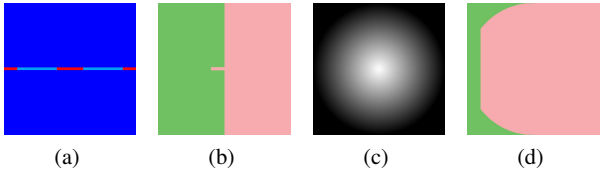


Fig. 4 Toy example. **a** Visualization of the sigmoid-metric color difference. **c** Average pixel saliency. **b,d** Corresponding seams.

Normally, $\kappa = 1/\epsilon$ will have a good practical performance, where ϵ is the width of bins of the histogram used in Ostu’s algorithm, which is set to 0.06 in our experiments.

The smoothness term is modified to

$$\tilde{S}_{p,q}(l_p, l_q) = \frac{1}{2}|l_p - l_q|(I_{\dagger}(p) + I_{\dagger}(q)), \quad (6)$$

$$I_{\dagger}(\cdot) = \text{sigmoid}(I_*(\cdot)), \quad (7)$$

where $I_{\dagger}(\cdot)$ denotes the sigmoid-metric color difference. As shown in Fig. 2c, $I_{\dagger}(\cdot)$ enforces the misalignment area more distinguishable from the alignment area than $I_*(\cdot)$ such that I_{\dagger} successfully avoids crossing the misalignment area.

2.2.2 Saliency weights

Fig. 4 shows another toy example where I_* is not perceptually best. In fact, the seams l_* and l_{\dagger} shown in **b** and **d** both cross the local misalignment area. Though the energy of I_{\dagger} is greater, it is perceptually better than I_* in aspect of the human perception since the location where the artifact arises is less remarkable than I_* .

In particular, the perception of image contents is nonuniform, which means that the human eye inclines to pay more attention to the salient objects. Thus, the artifact in the salient region is more remarkable than the one in the non-salient region.

In order to benefit from these observations, we define a saliency weight

$$W_{p,q} = \begin{cases} 0, & \text{if } p|q \in \partial_{\#}\mathbf{P}, \\ 1 + \frac{\omega(p)+\omega(q)}{2}, & \text{otherwise,} \end{cases} \quad (8)$$

where $\omega(\cdot)$ denotes the average pixel saliency of \mathbf{P} (Fig. 2d). We normalize $W_{p,q}$ into the range of $[1, 2]$ for avoiding overpenalizing. Because the final panoramas are usually cropped into rectangles in consumer-level photography, we optionally set $W_{p,q}$ to 0 if either p or q is located in the common border $\partial_{\#}\mathbf{P}$ of the canvas and \mathbf{P} (green line in Fig. 2a).

The perception-based energy function is defined as

$$\tilde{E}(l) = \sum_{p \in \mathbf{P}} D_p(l_p) + \sum_{(p,q) \in \mathbf{N}} W_{p,q} \cdot \tilde{S}_{p,q}(l_p, l_q), \quad (9)$$

where $W_{p,q}$ rises the penalty of $\tilde{S}_{p,q}(l_p, l_q)$ according to $\omega(\cdot)$. Fig. 2f shows that the endpoints of the seam have more freedom on $\partial_{\#}\mathbf{P}$ than the seam shown in Fig. 2e.

2.3 Proposed Seam-cutting Framework

Our seam-cutting framework is summarized in Algorithm 1.

Algorithm 1 Perception-based seam-cutting framework.

Input: An overlapping region \mathbf{P} of aligned images I_0 and I_1 .

Output: A stitching result.

1. Calculate $I_*(\mathbf{P})$ in Eq. 4;
 2. Calculate τ in Eq. 5 via Ostu’s algorithm [27];
 3. Calculate $I_{\dagger}(\mathbf{P})$ in Eq. 7 and $\tilde{S}_{p,q}$ in Eq. 6;
 4. Calculate $\omega(\mathbf{P})$ via salient object detection [38] and $W_{p,q}$ in Eq. 8;
 5. Calculate $D_p(\mathbf{P})$ in Eq. 2;
 6. Minimize $\tilde{E}(l)$ in Eq. 9 via graph-cut optimization [3], and blend I_0 and I_1 via gradient domain fusion [28].
-

3 Experiments

In our experiments, we first use SIFT [25] to detect and match features from the input images and use RANSAC [14] to determine a global homography warp for aligning them. Then, for the overlapping region, we use Ostu’s algorithm [27] to estimate the threshold τ and use the salient object detection [38] to calculate the pixel saliency weight. Finally, we use the graph-cut optimization [3] to obtain the seam and blend the aligned images via gradient domain fusion [28] to create a mosaic.

We compare our approach with the conventional seam-cutting approach and other mature stitching tools including AutoStitch [4, 5] and Microsoft ICE¹. For the sake of fairness, stitching results of the conventional and our perception-based seam-cutting approaches are based on the same homography alignment. The comparisons are done on our own dataset as well as public available datasets including Parallax [36] and SEAGULL [23].

Fig. 5 shows an illustrated example in [36]. Input images have parallax, which can be seen from the flowerpot. AutoStitch suffers from ghosting artifacts, Microsoft ICE and the conventional seam-cutting approach cannot create plausible results either. Visual artifacts are shown in red rectangle. Our method creates an artifacts-free result that is comparable to Parallax and SEAGULL.

Fig. 6 shows another illustrated example in [36]. Input images have parallax, which can be observed from the model plane. AutoStitch suffers from ghosting artifacts, Microsoft ICE and the conventional seam-cutting approach suffer from structure inconsistency. Visual artifacts are shown in red rectangle. Our method creates an artifacts-free result that is comparable to Parallax and SEAGULL.

¹ <http://research.microsoft.com/en-us/um/redmond/groups/ivm/ice>

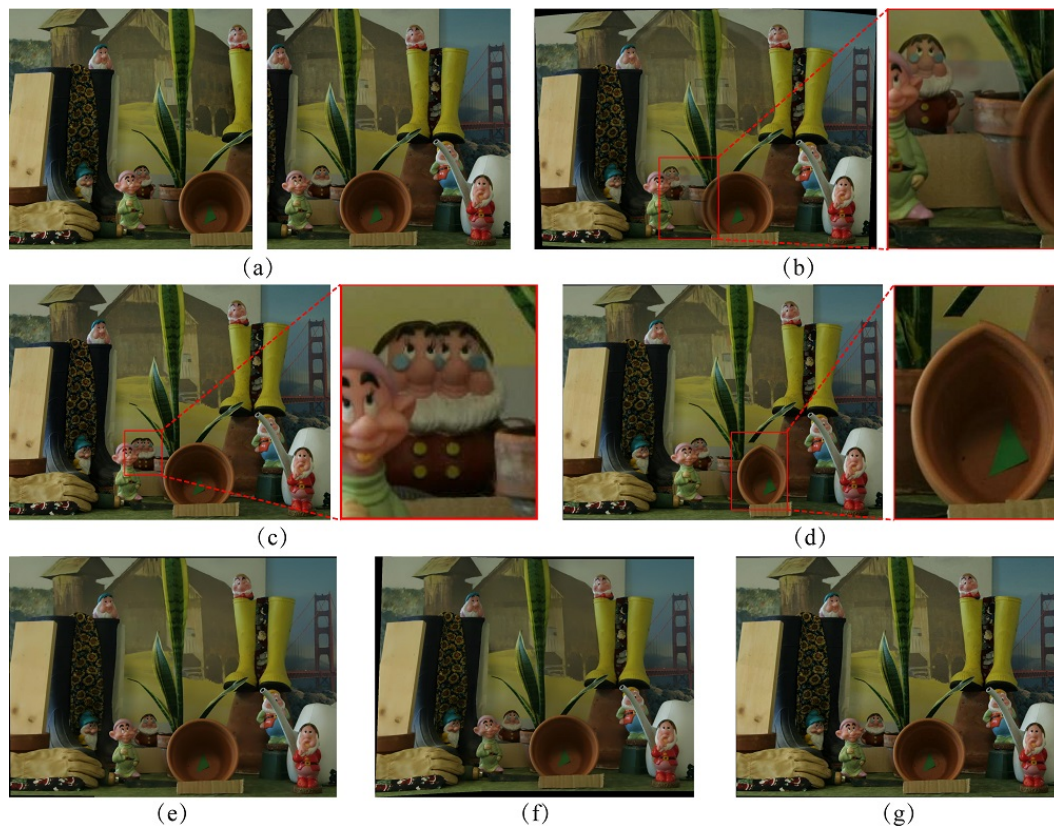


Fig. 5 Comparison between different stitching methods. **a** Input images. **b** AutoStitch. **c** Microsoft ICE. **d** Conventional seam-cutting approach. **e** Parallax. **f** SEAGULL. **g** Our method.

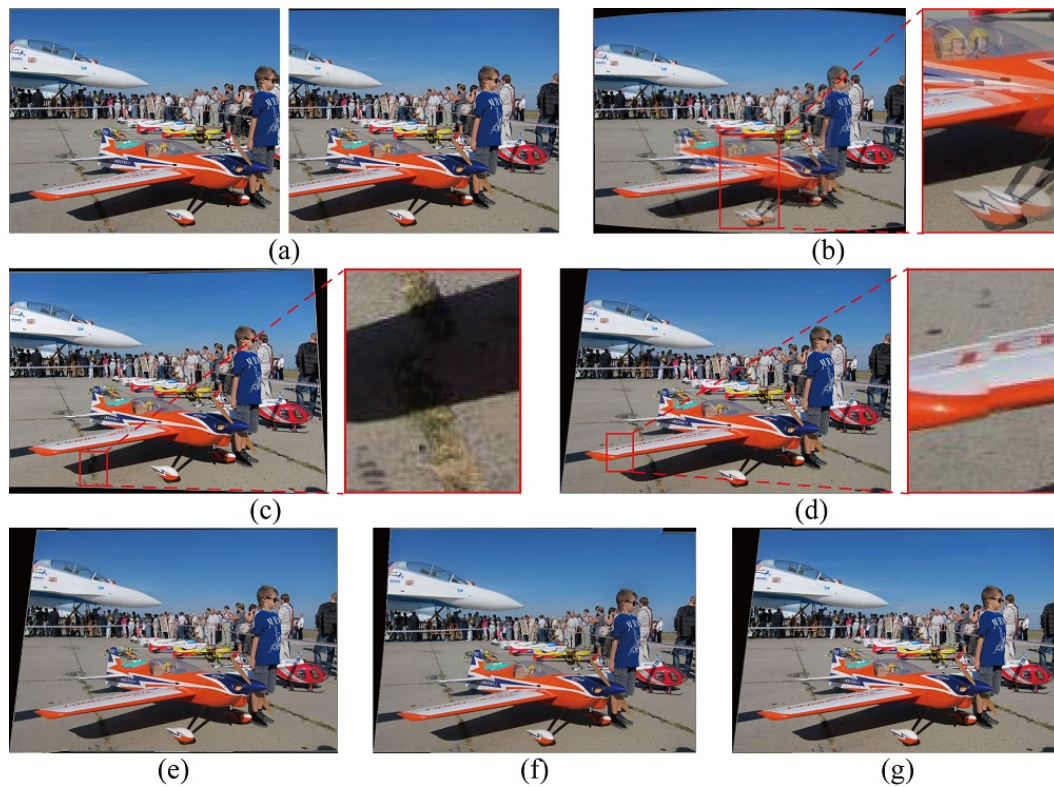
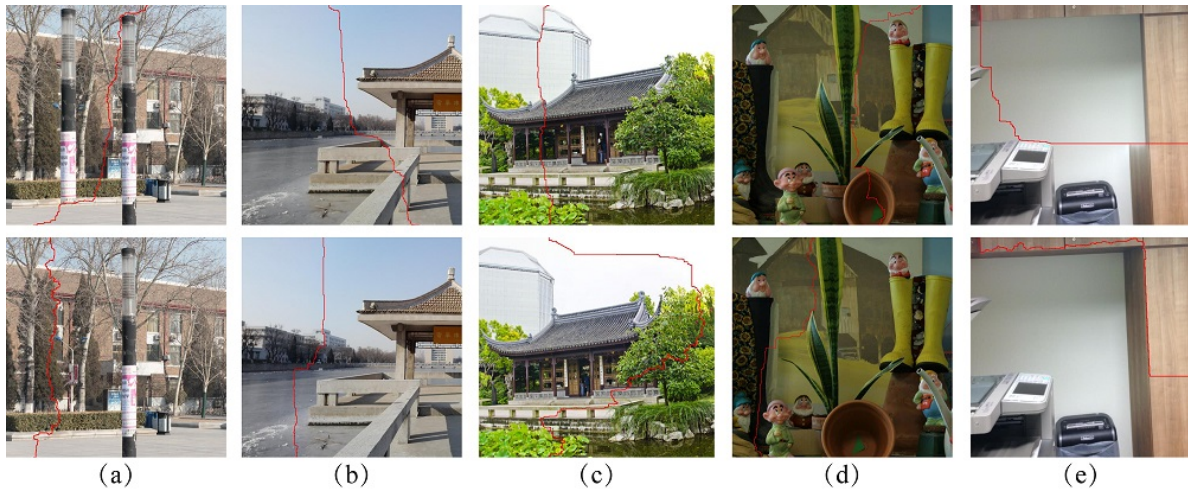
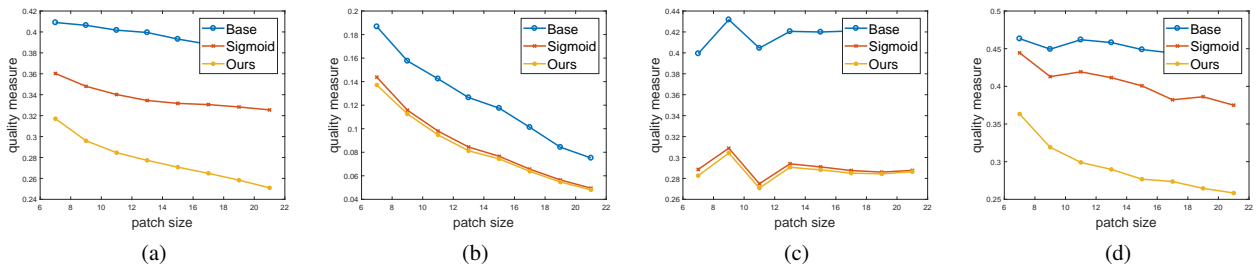


Fig. 6 Comparison between different stitching methods. **a** Input images. **b** AutoStitch. **c** Microsoft ICE. **d** Conventional seam-cutting approach. **e** Parallax. **f** SEAGULL. **g** Our method.

Table 1 Seam quality of the conventional seam-cutting approach, the one that only uses the sigmoid metric and ours.

No.	01.	02.	03.	04.	05.	06.	07.	08.	09.	10.
Base	0.393	0.290	0.209	0.078	0.179	0.209	0.118	0.390	0.270	0.284
Sigmoid	0.332	0.170	0.186	0.086	0.163	0.201	0.077	0.393	0.225	0.304
Ours	0.271	0.231	0.188	0.077	0.156	0.174	0.074	0.234	0.307	0.253

No.	11.	12.	13.	14.	15.	16.	17.	18.	19.	20.
Base	0.203	0.420	0.296	0.395	0.349	0.320	0.228	0.376	0.366	0.449
Sigmoid	0.209	0.291	0.252	0.362	0.284	0.259	0.240	0.345	0.180	0.401
Ours	0.179	0.288	0.252	0.352	0.284	0.240	0.172	0.335	0.195	0.277

**Fig. 7** Comparison between ‘Base’ and ‘Ours’. Top: ‘Base’. Bottom: ‘Ours’.**Fig. 8** Seam quality of different patch size. **a, b, c, d** correspond to 01, 07, 12, 20 in Table 1.

In Fig. 5 and 6, the input images and the fourth stitching results are from the project website of Parallax² and the fifth stitching results are from the project website of SEAGULL³. It is worth to note that, even without the advanced local alignment as in Parallax and SEAGULL, the combination of the global homography alignment and our perception-based seam-cutting approach can still produce comparable stitching results.

² <http://web.cecs.pdx.edu/~fliu/project/stitch/>

³ <http://www.linkaimo.com/publications/ImageStitching/ImageStitching.html>

3.1 Quantitative assessment

In the composition stage, a visible seam may produce *structure inconsistency* visual artifacts [33] (Fig. 5 and 6). We utilize the assessment strategy in [23] to quantitatively measure the seam’s performance. Specifically, for each pixel p_i on the stitching seam, we extract a $m \times m$ local patch (in pixels) centered at p_i . Then, we calculate the zero-normalized cross-correlation score (ZNCC) between the local patch in

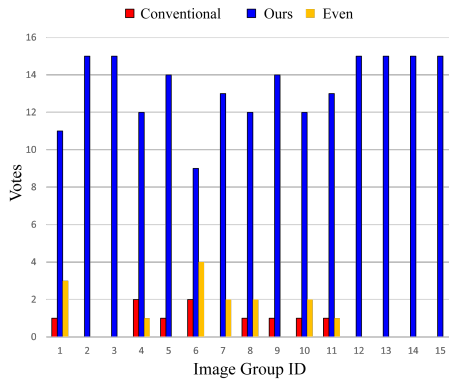


Fig. 9 Result of user study. Red indicates ‘Base’ wins. Blue indicates ‘Ours’ wins. Yellow indicates an even.

the target image and that in the reference image. Finally, along the seam, we define the quality measure as

$$M(seam) = \frac{1}{N} \sum_{i=1}^N \left(1 - \frac{ZNCC(p_i) + 1}{2} \right), \quad (10)$$

where N is the total number of pixels on the seam.

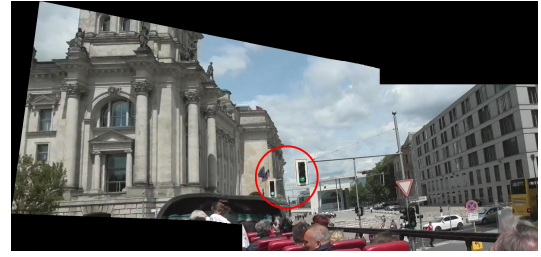
Now we use the quality measure to quantitatively compare the conventional and our perception-based seam-cutting approaches. We test the two methods on 20 groups of images including 8 from our own dataset and 12 from the public available datasets of Parallax [36] and SEAGULL [23]. Table 1 shows the comparison result between the conventional approach (‘Base’) and our approach (‘Ours’). We also compare the result of the seam-cutting approach that only uses the sigmoid metric (‘Sigmoid’, set $W_{p,q} := 1$ in Eq. 9). A smaller value usually indicates a perceptually better stitching seam and a more plausible stitching result.

In most of the cases, the seam quality of our approach is better than the one that only uses the sigmoid metric and both are better than the conventional one. In some examples (i.e. 02, 03, 09, 19), the seam qualities of the approach that only uses the sigmoid metric are slightly better than ours, but the stitching results are all visually plausible. We show a comparison of the stitching results (01, 02, 12, 14, 19) with significantly improved seam quality in Fig. 7. All 20 groups of examples are provided in the supplementary material including the intermediate seam result and the final stitching result of three methods.

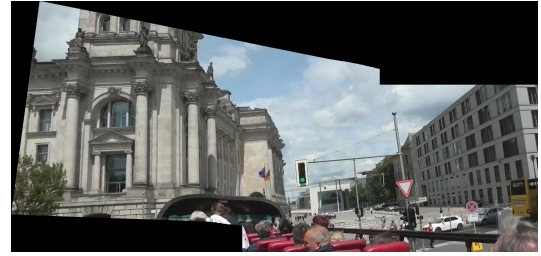
We experimentally find that the quality measure is stable in a reasonable range of m (Fig. 8). Here we set m to 15 in our experiments.

3.2 Subjective assessment

In order to investigate whether our proposed method is more consistent with the human perception, we conduct a user study to compare the conventional and our perception-based



(a)



(b)

Fig. 10 Integration with APAP. **a** ‘Base’. **b** ‘Ours’. Artifacts are indicated in red circle.

seam-cutting approaches. We invite 15 participants to rank 15 unannotated groups of stitching results (make a choice from 3 options: 1. A is better than B, 2. B is better than A, 3. A and B are even). Fig. 9 shows the result, which demonstrates that our stitching results win most users’ favor. All 15 groups of examples are provided in the supplementary material.

3.3 Integration

Besides the homography alignment, our proposed approach can be easily integrated with other advanced alignment. Fig. 10 shows an example from Parallax [36]. Given the overlapping region of the aligned images by APAP [34], our perception-based seam-cutting approach successfully creates an artifacts-free result while the conventional one fails.

4 Conclusion

In this paper, we propose a perception-based seam-cutting approach to handle image stitching challenges in consumer-level photography. Experiments show that our method outperforms the conventional seam-cutting approach. A comprehensive evaluation including quantitative and subjective assessment demonstrates that our results are more consistent with the human perception. In the future, we plan to generalize our method in the seam-driven framework to deal with the image alignment.

Acknowledgements This work is supported by Natural Science Foundation of China (No. 11626250).

References

1. Agarwala, A., Dontcheva, M., Agrawala, M., Drucker, S., Colburn, A., Curless, B., Salesin, D., Cohen, M.: Interactive digital photomontage. *ACM Transactions on Graphics* **23**(3), 294–302 (2004)
2. Boykov, Y., Kolmogorov, V.: An experimental comparison of min-cut/max-flow algorithms for energy minimization in vision. *IEEE Trans. Pattern Anal. Mach. Intell.* **26**(9), 1124–1137 (Sept. 2004)
3. Boykov, Y., Veksler, O., Zabih, R.: Fast approximate energy minimization via graph cuts. *IEEE Trans. Pattern Anal. Mach. Intell.* **23**(11), 1222–1239 (Nov. 2001)
4. Brown, M., Lowe, D.G.: Automatic panoramic image stitching using invariant features. *Int. J. Comput. Vision* **74**(1), 59–73 (2007)
5. Brown, M., Lowe, D.G., et al.: Recognising panoramas. In: *ICCV*, vol. 3, p. 1218 (2003)
6. Burt, P.J., Adelson, E.H.: A multiresolution spline with application to image mosaics. *ACM Transactions on Graphics* **2**(4), 217–236 (1983)
7. Chang, C.H., Sato, Y., Chuang, Y.Y.: Shape-preserving half-projective warps for image stitching. In: *Proc. IEEE Conf. Comput. Vision Pattern Recognit.*, pp. 3254–3261 (2014)
8. Chen, Y.S., Chuang, Y.Y.: Natural image stitching with the global similarity prior. In: *Proc. 14th Eur. Conf. Comput. Vision*, pp. 186–201 (2016)
9. Davis, J.: Mosaics of scenes with moving objects. In: *Proc. IEEE Conf. Comput. Vision Pattern Recognit.*, pp. 354–360 (1998)
10. Duplaquet, M.L.: Building large image mosaics with invisible seam lines. In: *Aerospace/Defense Sensing and Controls*, pp. 369–377. International Society for Optics and Photonics (1998)
11. Eden, A., Uyttendaele, M., Szeliski, R.: Seamless image stitching of scenes with large motions and exposure differences. In: *Proc. IEEE Conf. Comput. Vision Pattern Recognit.*, vol. 2, pp. 2498–2505 (2006)
12. Efros, A.A., Freeman, W.T.: Image quilting for texture synthesis and transfer. In: *Proceedings of the 28th Annual Conference on Computer Graphics and Interactive Techniques, SIGGRAPH '01*, pp. 341–346. ACM (2001)
13. Fang, X., Zhu, J., Luo, B.: Image mosaic with relaxed motion. *Signal, Image and Video Processing* **6**(4), 647–667 (2012)
14. Fischler, M.A., Bolles, R.C.: Random sample consensus: a paradigm for model fitting with applications to image analysis and automated cartography. *Commun. ACM* **24**(6), 381–395 (1981)
15. Gao, J., Kim, S.J., Brown, M.S.: Constructing image panoramas using dual-homography warping. In: *Proc. IEEE Conf. Comput. Vision Pattern Recognit.*, pp. 49–56 (2011)
16. Gao, J., Li, Y., Chin, T.J., Brown, M.S.: Seam-driven image stitching. *Eurographics* pp. 45–48 (2013)
17. Gracias, N., Mahoor, M., Negahdaripour, S., Gleason, A.: Fast image blending using watersheds and graph cuts. *Image and Vision Computing* **27**(5), 597–607 (2009)
18. Jia, J., Tang, C.K.: Image stitching using structure deformation. *IEEE Trans. Pattern Anal. Mach. Intell.* **30**(4), 617–631 (Apr. 2008)
19. Kolmogorov, V., Zabih, R.: What energy functions can be minimized via graph cuts? *IEEE Trans. Pattern Anal. Mach. Intell.* **26**(2), 147–159 (Feb. 2004)
20. Kwatra, V., Schödl, A., Essa, I., Turk, G., Bobick, A.: Graphcut textures: image and video synthesis using graph cuts. *ACM Transactions on Graphics* **22**(3), 277–286 (2003)
21. Levin, A., Zomet, A., Peleg, S., Weiss, Y.: Seamless image stitching in the gradient domain. In: *Proc. 8th Eur. Conf. Comput. Vision*, pp. 377–389 (2004)
22. Lin, C.C., Pankanti, S.U., Ramamurthy, K.N., Aravkin, A.Y.: Adaptive as-natural-as-possible image stitching. In: *Proc. IEEE Conf. Comput. Vision Pattern Recognit.*, pp. 1155–1163 (2015)
23. Lin, K., Jiang, N., Cheong, L.F., Do, M., Lu, J.: Seagull: Seam-guided local alignment for parallax-tolerant image stitching. In: *Proc. 14th Eur. Conf. Comput. Vision*, pp. 370–385 (2016)
24. Liu, F., Gleicher, M., Jin, H., Agarwala, A.: Content-preserving warps for 3d video stabilization. *ACM Transactions on Graphics (TOG)* **28**(3), 44 (2009)
25. Lowe, D.G.: Distinctive image features from scale-invariant keypoints. *Int. J. Comput. Vision* **60**(2), 91–110 (2004)
26. Mills, A., Dudek, G.: Image stitching with dynamic elements. *Image and Vision Computing* **27**(10), 1593–1602 (2009)
27. Otsu, N.: A threshold selection method from gray-level histograms. *Automatica* **11**(285-296), 23–27 (1975)
28. Pérez, P., Gangnet, M., Blake, A.: Poisson image editing. *ACM Transactions on Graphics* **22**(3), 313–318 (2003)
29. Rzhanov, Y.: Photo-mosaicing of images of pipe inner surface. *Signal, Image and Video Processing* pp. 1–7 (2013)
30. Szeliski, R.: Image alignment and stitching: A tutorial. Technical Report MSR-TR-2004-92, Microsoft Research (2004)
31. Szeliski, R., Shum, H.Y.: Creating full view panoramic image mosaics and environment maps. In: *Proceedings of the 24th Annual Conference on Computer Graphics and Interactive Techniques, SIGGRAPH '97*, pp. 251–258. ACM Press/Addison-Wesley Publishing Co. (1997)
32. Xu, Z.: Consistent image alignment for video mosaicing. *Signal, Image and Video Processing* **7**(1), 129–135 (2013)
33. Yang, L., Tan, Z., Huang, Z., Cheung, G.: A content-aware metric for stitched panoramic image quality assessment. In: *The IEEE International Conference on Computer Vision (ICCV)* (2017)
34. Zaragoza, J., Chin, T.J., Tran, Q.H., Brown, M.S., Suter, D.: As-projective-as-possible image stitching with moving dlt. *IEEE Transactions on Pattern Analysis and Machine Intelligence* **7**(36), 1285–1298 (2014)
35. Zeng, L., Zhang, W., Zhang, S., Wang, D.: Video image mosaic implement based on planar-mirror-based catadioptric system. *Signal, Image and Video Processing* **8**(6), 1007–1014 (2014)
36. Zhang, F., Liu, F.: Parallax-tolerant image stitching. In: *Proc. IEEE Conf. Comput. Vision Pattern Recognit.*, pp. 3262–3269 (2014)
37. Zhang, G., He, Y., Chen, W., Jia, J., Bao, H.: Multi-viewpoint panorama construction with wide-baseline images. *IEEE Transactions on Image Processing* **25**(7), 3099–3111 (2016)
38. Zhang, J., Sclaroff, S., Lin, Z., Shen, X., Price, B., Mech, R.: Minimum barrier salient object detection at 80 fps. In: *Proc. IEEE Int. Conf. on Comput. Vision*, pp. 1404–1412 (2015)